
Finite element modeling of polycrystalline solids

Paul Dawson* — Armand Beaudoin** — Kapil Mathur***
Gorti Sarma*

* *Cornell University*

*Dept. of Mechanical and Aerospace Engineering
196 Theory Center, ITHACA - NY 14853, USA*

** *Reynolds Metals Company*

*** *Thinking Machines Corporation*

ABSTRACT. Anisotropy in the plastic flow of polycrystalline solids can be computed based on the slip characteristics of individual crystals and included in finite element formulations as the constitutive description of the material. A variety of approaches exist for merging finite element formulations and polycrystal plasticity, and depending on the intended application the two may have different relationships to each other. We summarize two regimes that we refer to as large and small scale applications and outline a finite element formulation for each. Examples of both large and small scale applications are presented and some important issues associated with the implementation of each are discussed.

RÉSUMÉ. L'anisotropie dans l'écoulement plastique de matériaux polycristallins peut être formulée à partir des caractéristiques de glissement dans les grains, et prise comme loi de comportement du matériau dans une modélisation par éléments finis. Diverses approches existent pour coupler des formulations par éléments finis et la plasticité polycristalline, se différenciant, selon les applications visées, par leur mise en œuvre. Nous proposons ici deux approches, pour les problèmes privilégiant respectivement une grande échelle et une petite échelle, et donnons une formulation par éléments finis pour chacune d'elles. Des exemples d'application, aux deux échelles, sont présentés et discutés, ainsi que quelques points importants de la mise en œuvre.

KEY WORDS : polycrystal plasticity, finite element method, metal forming, parallel computing.

MOTS-CLÉS : plasticité polycristalline, méthodes d'éléments finis, formage des métaux, calcul parallèle.

1. Introduction

The finite element method can be used in conjunction with polycrystal plasticity theory for modeling the anisotropic deformations of crystalline solids. Polycrystal plasticity provides a micromechanical model for slip dominated plastic flow and serves as a constitutive description of the material. The finite element method provides a numerical method for solving the partial differential equations associated with the balance laws for material motion. The two can be combined in different ways depending on the goals of a modeling effort.

One possibility is to embed polycrystal theory within a finite element formulation as a constitutive theory in much the same way as is currently done for continuum elastoplasticity models. For this purpose we refer to a crystal ensemble as an aggregate. An aggregate underlies a continuum point and is interrogated at appropriate times in a simulation to evaluate flow properties. In turn, hardening of crystal slip systems and crystal rotations follow from the continuum fields of stress and deformation. Polycrystal plasticity can be viewed in this context as a state variable constitutive theory in which the orientation distribution of crystal lattices, along with the crystal hardnesses, comprise the description of state. A second combination of finite elements and polycrystal plasticity is associated with more detailed study of the crystal ensembles themselves. In this case, finite elements discretize the crystals and balance laws are applied to form an idealization of the microstructure. For this case, a crystal ensemble is called a polycrystal. Within an element the single crystal relations hold, with the finite element solution providing insight into the distribution of deformation and details of load sharing in the polycrystal.

We will refer to these large and small scale applications, respectively. The two have many issues in common, including the effective methods for parallel computer architectures to exploit the concurrencies inherent with such models. However, there also are issues that are distinctly related to one application, or are much more important in one than the other. For small scale applications, the smoothness of properties cannot be assumed, as crystal interfaces exist and properties are not continuous across them. For large scale, the linking of micro and macro length scales arises through assumptions made in partitioning the deformation among crystals of an aggregate. The relationship between the dimensions of the aggregate and those of the body is a concern, but is not explicitly defined as in the small scale.

In this paper, we discuss finite element formulations for both small and large scale applications. We begin with a review of single crystal equations, which are common to both. We then present the small scale formulation, followed by that for the large scale. As an example of a small scale application, the deformation of an aggregate of hexagonal close-packed crystals is presented; for the large scale formulation we show an analysis of the limiting dome height test. We finish with a discussion of issues concerning the implementation of finite element formulations that utilize polycrystal plasticity as the constitutive representation.

2. Single Crystal Relations

The plastic flow is assumed to be a consequence of rate-dependent slip, occurring on a restricted number of slip systems and diffusely within the crystals [KOC 70]. From the velocity \mathbf{u} the required kinematic quantities associated with the deformation can be computed:

$$\text{grad } \mathbf{u} = \mathbf{L}^c = \mathbf{D}^c + \mathbf{W}^c, \quad (1)$$

where \mathbf{L}^c is the velocity gradient and \mathbf{D}^c and \mathbf{W}^c are the deformation rate and spin (the symmetric and skew parts of \mathbf{L}^c , respectively). The motion indicated by \mathbf{L}^c is accommodated by the crystal's slip systems through a combination of shear on the active systems and rotation of the lattice. This decomposition may be written as:

$$\mathbf{D}^c = \mathbf{D}^p \quad (2)$$

$$\mathbf{W}^c = \dot{\mathbf{R}}^* \mathbf{R}^{*T} + \mathbf{W}^p. \quad (3)$$

The deformation rate and spin in a frame that remains coincident with the lattice may be expressed as a linear combination of the slip motion occurring on the active systems:

$$\mathbf{D}^p = \sum_{\alpha} \mathbf{P}^{\alpha} \dot{\gamma}^{\alpha} \quad (4)$$

and

$$\mathbf{W}^p = \sum_{\alpha} \mathbf{Q}^{\alpha} \dot{\gamma}^{\alpha}. \quad (5)$$

\mathbf{P}^{α} and \mathbf{Q}^{α} are the symmetric and skew portions of the Schmid tensor, respectively, and α indicates a specific slip system. The Schmid tensor itself is constructed from the tensor product of the slip direction and the slip plane normal vectors. \mathbf{R}^* describes the rotation of the lattice frame with respect to a reference, so updating \mathbf{R}^* for every crystal according to equation [3] evolves the crystallographic texture.

On each slip system, the resolved shear stress τ^{α} is related to the shear rate through a relationship of the form:

$$\tau^{\alpha} = \mathbf{P}^{\alpha} \cdot \boldsymbol{\sigma}'^c = \hat{\tau} \left(\frac{\dot{\gamma}^{\alpha}}{a} \right)^m, \quad (6)$$

where $\boldsymbol{\sigma}'$ is the deviatoric Cauchy stress, $\hat{\tau}$ is the crystal hardness, $\dot{\gamma}^{\alpha}$ is the shear rate, and a and m are material parameters. This relation is an approximation to the actual dependency, which would include effects of temperature and more general rate dependency [ASA 85].

¹ A superscript c will refer to a crystal quantity for variables that are defined both at the crystal and aggregate (macroscopic) levels.

The hardness $\hat{\tau}$ evolves with straining according to a simple relationship that embodies a saturation hardness, τ_s , which depends on strain rate and temperature:

$$\dot{\hat{\tau}} = \Theta_0 \left(\frac{\hat{\tau} - \tau_0}{\tau_s - \tau_0} \right) \dot{\gamma}. \tag{7}$$

Here, $\dot{\gamma}$ is a net shear rate within the crystal, and Θ_0 , τ_0 , and n are material parameters. Equal hardening is assumed for all slip systems of the same type, neglecting any variations from differing levels of slip system activity. No attempt is made to quantify the dislocation structure in any detail, but rather diffuse slip is assumed to harden the crystal uniformly over its volume.

We can invert equation [6] to obtain the shearing rate on each slip system as:

$$\dot{\gamma}^\alpha = a \left(\frac{\tau^\alpha}{\hat{\tau}} \right)^{\frac{1}{m}}, \tag{8}$$

which can be substituted into equation [4]. Use of the relationship between the resolved shear stress and the deviatoric stress (equation [6]) along with equation [2] leads to a non-linear relation between the rate of deformation and the deviatoric stress in the crystal:

$$D^c = \left[\sum_\alpha \frac{a}{\hat{\tau}} \left(\frac{\tau^\alpha}{\hat{\tau}} \right)^{\frac{1}{m}-1} P^\alpha \otimes P^\alpha \right] \sigma'^c \tag{9}$$

or

$$D^c = \mathcal{M}^c \sigma'^c, \tag{10}$$

where \mathcal{M}^c is the crystal compliance tensor and is given by the expression in brackets in equation [9].

3. Small Scale Applications

Small scale applications are ones in which the crystal dimensions are comparable to the entire body. Finite elements typically have volumes similar to that of a single crystal, and in many cases the correspondence is one-to-one. In defining the mesh, one also is prescribing the topology of the polycrystal. Gradients of the deformation are permitted over an element, and thus over individual crystals as well. The balance laws are applied directly to a polycrystal via the weighted residuals of the finite element formulation. The solution to the field equations renders the partitioning of deformation among the crystals.

The single crystal anisotropy is the source both of interesting behaviors (and thus the focus of many studies) and of numerical difficulties in the solution of the model equations. For example, the nonuniformity of straining is

of particular importance. The tendency of deformations to localize into shear bands as the preferred mode of deformation has received considerable attention. Also, an understanding of crystal to crystal variations in the deformation and their influence on texture development is necessary for improvements to models which employ simpler mean field assumptions such as the Taylor or Sachs hypotheses. The discontinuity of properties across the elemental boundaries due to the single crystal anisotropy may cause difficulties. Conventional kinematically-based finite element formulations rely on increased resolution of the discretization to reduce traction discontinuities at elemental interfaces, and thereby approach convergence. However, since property discontinuities are an inherent feature of interfaces within a polycrystal, special attention to the element boundaries is necessary to assure converged solutions.

Small scale simulations were reported as early as 1978 by Gotoh [GOT 78], in which 125 face-centered cubic (FCC) crystals were modeled using a planar arrangement of elements. Gotoh studied the initial yielding of this assembly assuming that crystals uniformly covered orientation space and were randomly positioned in the mesh. Needleman, Asaro, Lemond and Peirce [NEE 85] implemented the rate dependent formulation in a large strain elastoplastic framework and studied the localization of thin strips comprised of crystals with planar slip modes. Harren and Asaro [HAR 89] studied the validity of the Taylor assumption using a similar formulation to Needleman *et al* [NEE 85]. McHugh, Asaro, and Shih [MCH 93] applied this formulation to the study of metal matrix composites, showing the effect of strain localization around harder phases on the overall mechanical response of the composite. Becker [BEC 91a] and Kalidindi, Bronkhorst and Anand [KAL 92] have performed similar studies, but applied full FCC deformation modes to the crystal kinematics, although the meshes were constrained to two-dimensional deformation modes (as intended to replicate plane strain compression). In both studies the polycrystal models were implemented as user defined material subroutines in a general purpose commercial finite element code. Becker [BEC 91b] examined a similar problem with the same formulation in his analyses of the strain distributions in the deformation zone of a thin sheet subjected to bending. Slip system activity has been investigated using finite elements by Havlicek, Tokuda, Hino, and Kratochvil [HAV 92] and by Yao and Wagoner [YAO 93].

3.1. Hybrid formulation

Hybrid formulations have been proposed [TON 69, ATL 75, BRA 83] as alternatives to the conventional kinematically-based finite element formulations. Within the context of a hybrid formulation, domain decomposition is applied to the polycrystal such that elements correspond to individual crystals [BEA 94]. The elements, or domain subdivisions, are constrained to be in mutual equilibrium by requiring that, in a weighted residual sense, the surface tractions vanish.

This constraint is written for all domains of the polycrystal²:

$$\sum_e \left[\int_{\Gamma_e} \Phi \cdot \mathbf{t}^e d\Gamma - \int_{\Gamma_i} \Phi \cdot \mathbf{t} d\Gamma \right] = 0, \quad (11)$$

where Φ are weights. The superscript and subscript e denote an elemental surface. The traction, \mathbf{t} , at any point on the boundary is related to the stress via the Cauchy formula:

$$\mathbf{t} = \boldsymbol{\sigma} \mathbf{n} = (\boldsymbol{\sigma}' - p\mathbf{I})\mathbf{n}, \quad (12)$$

where \mathbf{n} is the surface normal; p is the pressure; and \mathbf{I} is the identity tensor. Substitution of the Cauchy formula into the traction equilibrium residual gives after integration by parts:

$$\sum_e \left[\int_{\Omega_e} \text{tr}[(\boldsymbol{\sigma}' - p\mathbf{I}) \nabla \Phi] d\Omega - \int_{\Gamma_i} \Phi \cdot \mathbf{t} d\Gamma \right] = 0. \quad (13)$$

Assumption of isochoric plastic deformations requires that the divergence of the velocity vanish (neglecting elastic deformations), resulting in:

$$\text{div } \mathbf{u} = \text{tr } \mathbf{D} = \text{tr } \mathbf{D} = 0. \quad (14)$$

A second weighted residual is formed on this incompressibility constraint equation using weights \mathcal{P} :

$$\int_{\Omega} \mathcal{P} (\text{tr } \mathbf{D}) d\Omega = 0. \quad (15)$$

The crystal constitutive behavior is obtained from the relation between the rate of deformation and the deviatoric stress (equation [10]). A residual can be constructed using this equation together with appropriate weights, \mathbf{T}^c :

$$\int_{\Omega_e} \mathbf{T}^c \cdot (\mathcal{M}^c[\boldsymbol{\sigma}'] - \mathbf{D}) d\Omega = 0. \quad (16)$$

To estimate the crystal stiffness, \mathcal{M}^c , equation [10] is solved using the deformation rate corresponding to the previous iterate of the velocity field. This system renders an estimate for the stress for the prescribed deformation rate, but may be difficult to solve if the rate sensitivity is quite low. A Newton-Raphson procedure is employed with a line search algorithm to limit the revisions to the stress to ones that reduce the residual error. The first iteration begins at the stress vertex of the rate independent yield surface with maximum work. If the line search fails, a different vertex is used to begin the Newton iterations.

²For the small scale formulation presented here there is no distinction between the crystal and continuum scales, so the superscript c is not necessary.

Even for the more anisotropic crystals this procedure was successful for rate sensitivities as low as 0.005.

Trial functions are introduced in the residuals for the interpolated field variables. Using the hybrid formulation both the velocity and the stress (deviatoric and spherical portions) are represented with approximating functions:

$$\boldsymbol{\sigma}' = [N^\sigma]\{s^c\}; p = [N^p]\{P\}; \mathbf{u} = [N^u]\{U\}. \quad (17)$$

For the deviatoric stress, piecewise discontinuous functions are specified which satisfy equilibrium within an element *a priori* [BRA 83].

Each residual is written in matrix form using the trial functions. For the crystal slip relation, equation [16], nodal stresses are related to the nodal velocities:

$$[H^c]\{s^c\} - [R]^T\{U\} = 0. \quad (18)$$

(Matrix definitions are given in the Appendix.) The traction equilibrium residual is given by:

$$\sum_e \left[\sum_c [R]\{s^c\} - [G]\{P\} - \{f\} \right] = 0. \quad (19)$$

The nodal stresses can be eliminated by inverting equation [18] and then substituting the result into equation [19]. This yields:

$$\sum_e \left[\sum_c [R][H^c]^{-1}[R]^T\{U\} - [G]\{P\} - \{f\} \right] = 0. \quad (20)$$

This equation is solved simultaneously with the discretized residual for the incompressibility constraint:

$$[G]^T\{U\} = 0, \quad (21)$$

to give the velocity field for the polycrystal corresponding to its current geometry and state. Special attention is needed in solving this system using the conjugate gradient method due to the poor conditioning resulting from the incompressibility constraint [BEA 93]. The geometry and state are then advanced over a time increment by Euler integration of the coordinate velocities and the evolution equations for the lattice orientations and hardnesses.

3.2. Simulation of small-scale processes

Plane strain compression is frequently chosen for detailed study because it is an idealization of flat rolling (in which large strains may be accomplished)

and because a great deal is understood concerning the behavior of materials under this loading. Model results can be compared readily either to the extensive body of experimental data for many materials or to the predictions of other models. The response of materials comprised of hexagonal close-packed (HCP) crystals under plane strain compression has been examined using this approach [DAW 94], and the results are summarized here.

The material is viewed as a polycrystal in that the macroscopic response is the average response of a population of single crystals. By discretizing the microstructure crystal-by-crystal we can permit individual crystals to respond independently, constrained by balance laws and compatibility. The anisotropy of the crystal, together with the differences in orientation between neighboring crystals, leads to nonuniformity in the deformation field over the polycrystal. The nonuniformity stems from the kinematic degrees of freedom associated with the finite element discretization. These results can be compared to those obtained by making a more restrictive, but more easily implemented, assumption of uniform straining among all crystals that comprise the polycrystal (e.g. a Taylor assumption). The textures computed by these two approaches differ due to the local deviations from plane strain compression that are permitted with the discretized microstructure. This approach has been used to model FCC polycrystals, and has shown that the inhomogeneity in strains from crystal to crystal leads to the development of the brass component of texture under plane strain compression [BEA 94]. In the following discussion we describe the HCP system, the manner in which a discretized microstructure is constructed, and the trends that appear for increasing degree of single crystal anisotropy.

HCP crystals [HON 84] often are categorized by the axial ratio ($\frac{c}{a}$ ratio, in the commonly used terminology). Here, we specify an axial ratio of 1.63, corresponding to the ideal value for packing but not representing a specific metal. Basal and prismatic slip systems are assumed to be the principal contributors to the crystal deformations. Pyramidal slip also may occur on the $\{11\bar{2}1\} < \bar{1}123 >$ slip systems [HUT 77, TOM 91]. In the simulations performed the strength of these systems relative to the prismatic and basal systems (which were taken as equal) was varied from unity to ten. In all cases the rate sensitivity, m , was held fixed at 0.10, a value appropriate to higher temperatures where twinning is not an important contribution. To preserve the relative strength ratios with deformation, no slip system hardening was permitted.

A sample of material is constructed from three dimensional brick elements, each consisting of an individual crystal. For the sample to be truly representative of a real material, the number of crystals must be relatively large. In the examples that follow, 1000 elements form a polycrystal. The mesh used in the simulations, however, has 4096 elements with 16 elements in each of the three coordinate directions. The polycrystal is the inner 1000 elements of this mesh, leaving a layer of elements three elements thick around the outer surface that act as an effective medium through which the boundary conditions are imposed on the polycrystal. The lattice orientations of all crystals are assigned from an original orientation distribution which was close to uniform.

Some initial texture was present, which caused the asymmetry in the textures shown later. A specific orientation is chosen randomly for each element from the distribution.

The finite element polycrystal was subjected to boundary velocities corresponding to plane strain compression. The global coordinate directions are associated with the rolling process as: compression - normal (ND); extension - rolling (RD); and the out-of-plane - transverse (TD). A total of 100 equal time steps were imposed in order to reduce the polycrystal to one half of its original height. This produced a natural axial strain ϵ_{11} of 0.69, which corresponds to an effective strain ($\bar{\epsilon} = \sqrt{\frac{2}{3}\epsilon_{ij}\epsilon_{ij}}$) of 0.8. The initial lattice orientation changes with straining for each crystal; the spin terms needed to compute the reorientation were evaluated at the centroid of the element. When the mesh distortion

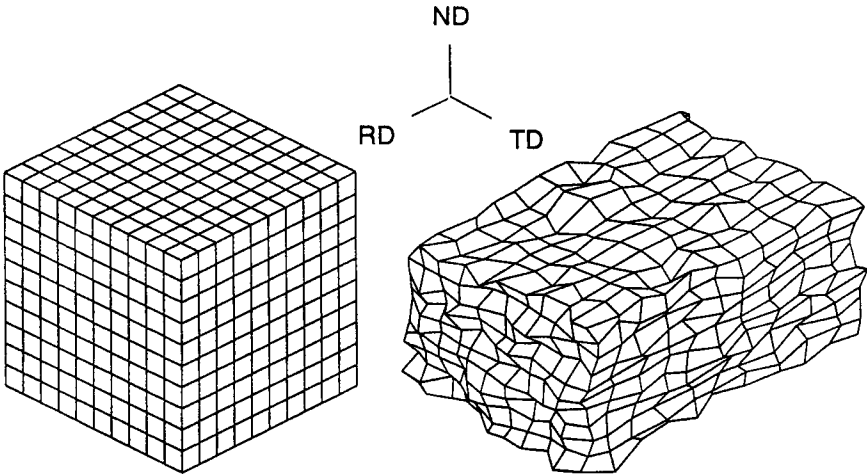


Figure 1: Initial and deformed finite element meshes for HCP polycrystal.

became severe, a mesh was repaired by replacing the distorted elements with regular ones having the same aspect ratio as the overall polycrystal. The lattice orientations before repair were preserved after repair. The variability of straining among the elements/crystals is quite evident from the deformed mesh for the case where pyramidal strength is five times the basal strength as shown in Figure 1.

The ratio of the pyramidal strength to basal/prismatic strength (relative pyramidal strength or RPS) was parametrically varied in the set of simulations performed. Beginning with the rather unrealistic case of RPS equaling unity, its value was increased to three, five, and finally ten. Two simulations were conducted for each value of RPS: one being the finite element polycrystal and the other being a Taylor model computation. As mentioned previously, the

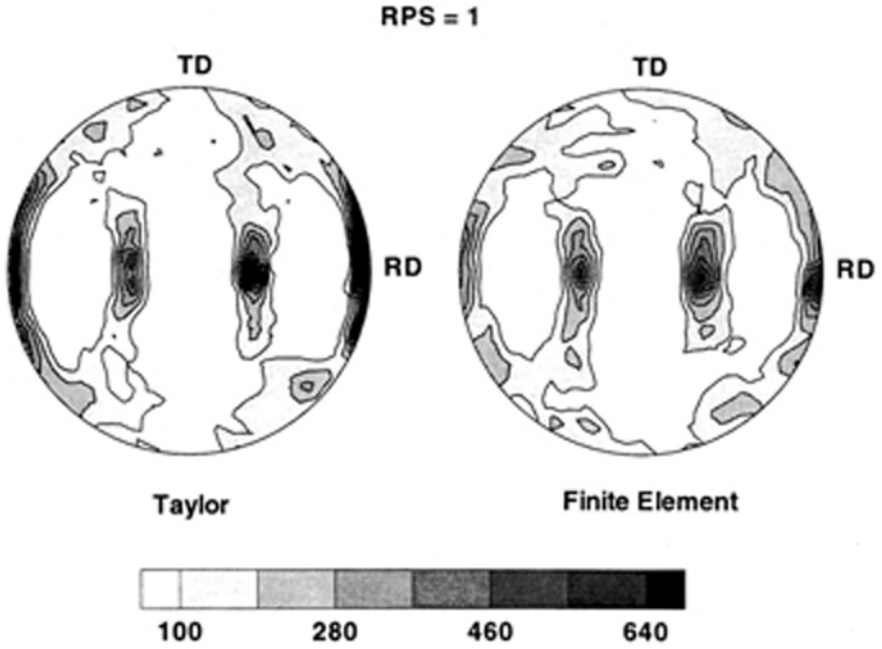


Figure 2: $\langle 0001 \rangle$ pole figures from the Taylor and finite element models for the case of RPS = 1. Plane strain compression; effective strain of 0.8.

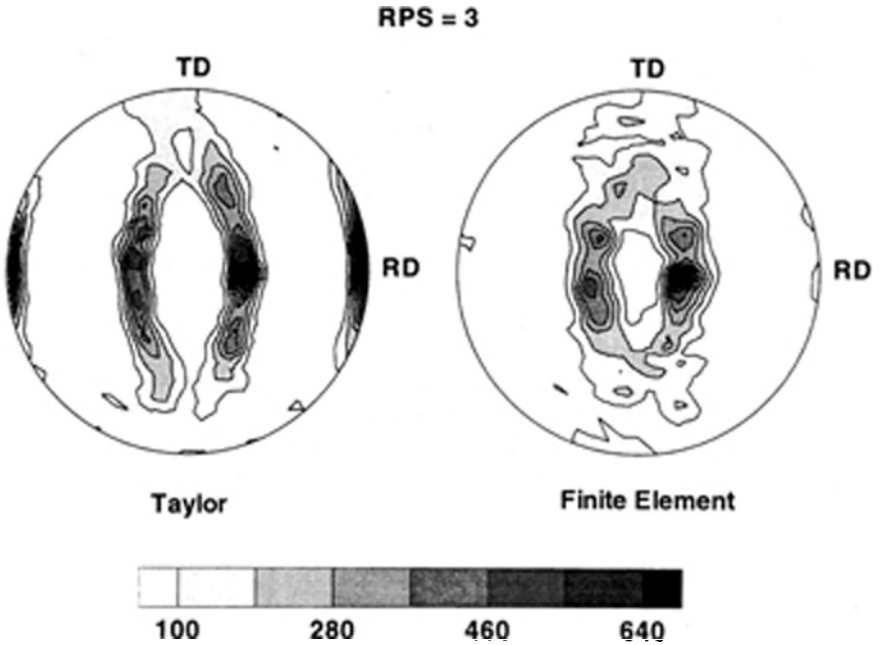


Figure 3: $\langle 0001 \rangle$ pole figures from the Taylor and finite element models for the case of RPS = 3. Plane strain compression; effective strain of 0.8.

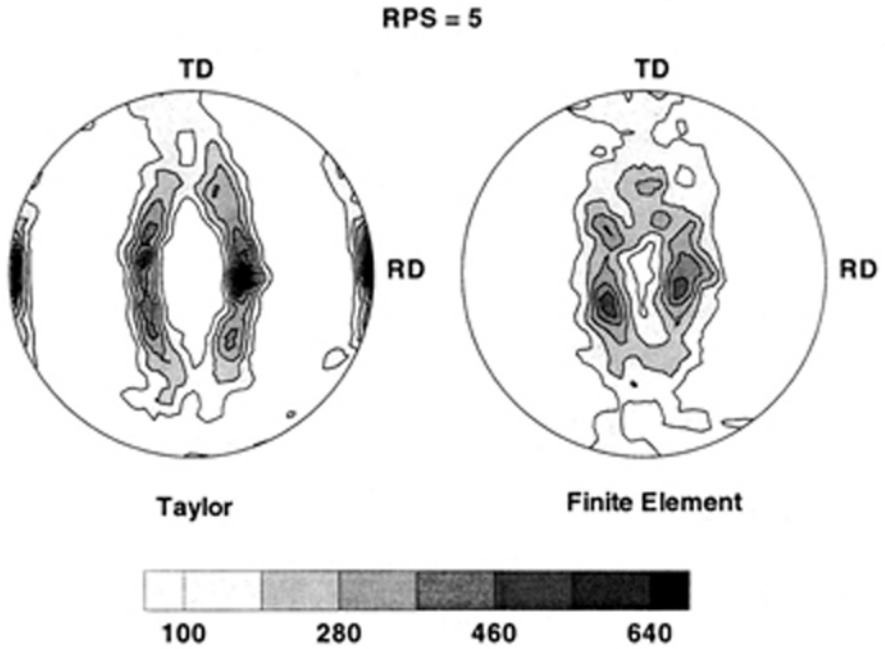


Figure 4: $\langle 0001 \rangle$ pole figures from the Taylor and finite element models for the case of $RPS = 5$. Plane strain compression; effective strain of 0.8.

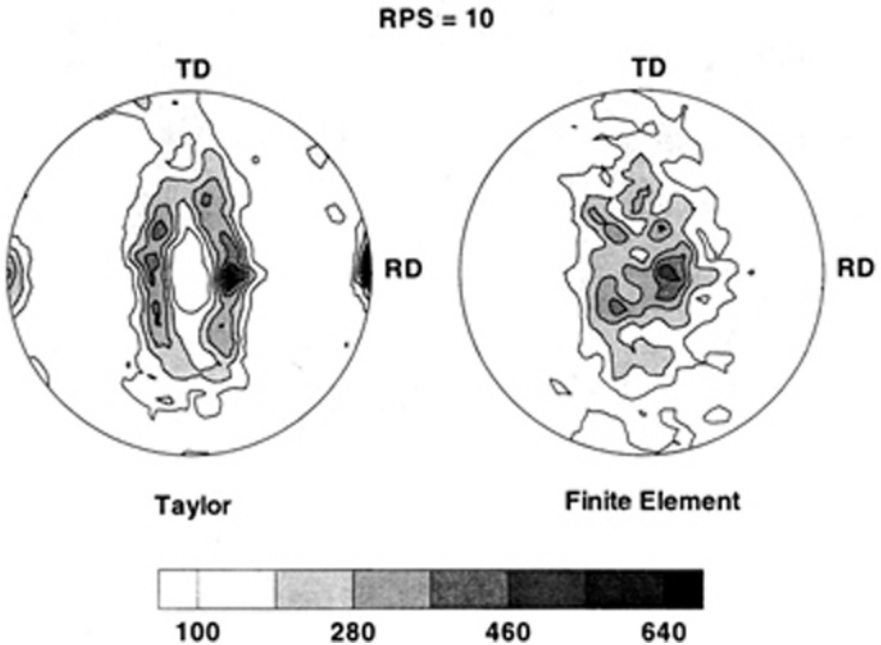


Figure 5: $\langle 0001 \rangle$ pole figures from the Taylor and finite element models for the case of $RPS = 10$. Plane strain compression; effective strain of 0.8.

Taylor computation imposes equal straining on all crystals of the polycrystal. Figures 2 to 5 give $\langle 0001 \rangle$ pole figures for each model for values of the RPS corresponding to 1, 3, 5, and 10, respectively. The principal features of the texture, especially for RPS values of 5 and 10, correspond generally to that reported for Zr 2.5%Nb rolled at elevated temperature [LEB 94].

Several trends are apparent. In every case the textures derived from the finite element simulations are more diffuse than the corresponding Taylor computation. The more diffuse texture coincides with the greater variability in straining experienced as the RPS increases. As the RPS becomes higher, each HCP crystal in essence inherits an inextensible direction along its lattice prismatic axis. This makes it less likely that crystal deformations will coincide with the macroscopic value since each crystal becomes incapable of a full range of deformation modes. Thus the qualitative differences between the Taylor and

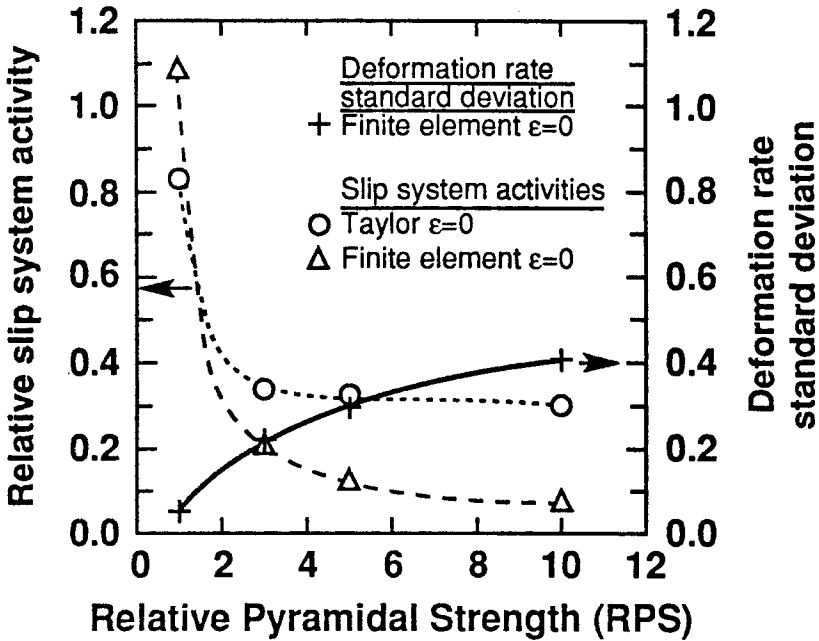


Figure 6: Slip system activities and deformation rate standard deviations for polycrystals having various relative pyramidal strengths.

finite element polycrystal predictions emerge. As shown in Figure 6, the Taylor model continues to utilize the pyramidal systems even when the RPS is high because those systems offer the only means for extension along the prismatic axis. The finite element polycrystal exhibits greater crystal to crystal strain

variations as it prefers to shift straining to more favorably oriented crystals than to force the strong pyramidal systems to be active. This is quantitatively substantiated by the increasing value of the standard deviation of the shearing deformation rate component in the plane containing the transverse and rolling directions with increasing RPS value. This has a very substantial impact on the texture development, as is evident from Figure 5.

4. Large Scale Applications

Large scale applications are those in which the body, herein called the workpiece, is very much larger than individual crystals. Examples include the rolling of plates, sheet forming, and forging. A variety of technical issues arise as the focus of these applications, such as unsymmetric deformations (earing), texture gradients within the workpiece (and consequential effects on mechanical properties), macroscopic shear banding, and residual stresses.

Finite element formulations require the material response as part of the integration of elemental stiffness and force matrices arising from the residual on the balance of linear momentum. Polycrystal plasticity provides a microstructurally motivated constitutive model for the flow which defines the yield condition and flow rule for a material element comprised of an aggregate of crystals. The distribution of lattice orientations, along with the hardness of the crystals, defines the material state. The balance laws are not applied to the crystals of the aggregate *per se*, but rather the aggregate is interrogated to define the stress and flow properties (as needed to evaluate the stiffness). Constitutive assumptions, such as a Taylor hypothesis or self consistent theories, are made in deciding how to project the macroscopic deformation onto the crystals of an aggregate and subsequently to average the resulting responses (stresses) of those crystals to obtain a macroscopic value.

The rolling of plate and drawing of wire using an Eulerian formulation were reported by Mathur, Dawson, and Kocks [MAT 89, MAT 90a, MAT 90b] using both Taylor and relaxed constraints assumptions for aggregates comprised of FCC crystals. Here the material was assumed to have an initially uniform orientation distribution, and texture gradients in the products were predicted. van Bael, van Houtte, Aernoudt, Hall, Pillinger, Hartley, and Sturgess [VAN 91] have implemented a procedure for computing the anisotropic stiffness from an approximation to the average Taylor factor written using a series expansion of terms involving the strain rate. The expansion parameters may be computed from the texture and thus updated with continued deformation. They have implemented the model in a Lagrangian elastoplastic formulation and simulated rolling of BCC metals. Kalidindi, Bronkhorst and Anand [KAL 92] reported on the implementation of a polycrystal model based on Taylor assumption into a commercial elastoplastic displacement-based code. They compared the textures computed to those measured for laboratory microforgings of copper. Chastel and Dawson [CHA 91, DAW 93] modeled the

rolling of initially textured silicon steels with an Eulerian formulation using a model for pencil glide slip modes. Detailed comparisons of through thickness texture variations were made with experiment. Chastel, Dawson, Wenk and Bennett [CHA 93b] used the same Eulerian viscoplastic formulation to study texturing of rocks in the earth's mantle. Here, because of low crystal symmetry an equilibrium based model was employed to partition the deformation among crystals of an aggregate [CHA 93a]. Comparisons were made between computed and measured seismic velocities through the mantle. Maniatty [MAN 91] extended this Eulerian viscoplastic formulation to include elasticity and examined the influence of initial texture on the residual stress distribution in the product. Smelser and Becker [SME 91] have studied drawing of cups with a commercial code that calls the polycrystal theory through a user defined module, both using single crystal and polycrystal representations.

Recent progress in parallel computing has been exploited for large scale applications. Parallel computing hardware, together with rewriting of algorithms for this architecture, have made it possible to simulate 3-D deformations involving several thousand elements each with hundreds of crystals defining every aggregate. For example, Beaudoin, Mathur, Dawson and Johnson [BEA 93] examined the evolution of texture in compression test specimens; hydroforming was studied by Dawson, Beaudoin, Mathur, Kocks and Korzekwa [DAW 92a, DAW 92b] with respect to the formation of ears. The hydroforming simulation demonstrated the ability to predict both the location and strength of ears in the initially textured aluminum sheet.

4.1 Linking micro and macro length scales

In applying polycrystal plasticity, it is assumed that the properties at any point in the sheet are determined from a collection of anisotropic crystals that underlies that point. The modes of the crystal deformation are set by the slip system geometry, given that slip is the dominant deformation mechanism and other mechanisms can be neglected (including twinning, grain boundary sliding, and diffusion). An assumption, or rule, is employed to partition the macroscopic (average) strain among the individual crystals within an aggregate. A variety of rules are possible, some of which constitute bounds. By modeling the linkage between the microscopic (crystal) and macroscopic (continuum) scales with partitioning rules, the need to define each crystal's neighbors is circumvented. Instead, the aggregate of crystals can be thought of as a set of co-existing orientations whose averaged responses define the macroscopic properties. The orientations play the role of state variables, together with the crystal strengths and the grain shape. As state variables, the orientations replace the need to remember the deformation path, but require initialization to begin an analysis.

Several different assumptions which are commonly used to link the microscopic and macroscopic length scales and to provide a means to partition the

deformations and the stresses among the crystals of an aggregate are discussed here. For high symmetry crystals such as BCC crystals, and when the crystals are nearly equiaxed, it often is assumed that each crystal of the aggregate experiences the same rate of deformation. This partitioning rule (referred to as the Taylor assumption) is extended to include the spin, so the crystal velocity gradient is common to all crystals [ASA 85]. However, heavily worked crystals can become flat and elongated. Then, based on the aspect ratio of the grains (as computed using the principal stretches of the macroscopic deformation gradient), some crystals within an aggregate are subjected to relaxed kinematic constraints [HON 78, TOM 84]. For these crystals the continuity of the tractions and displacements is imposed based on the orientation of the largest interface between crystals. Given that each crystal deforms homogeneously, this leads to a mixed combination of stress and deformation constraints between crystals of an aggregate.

Stated in terms of the crystal kinematics, the extended Taylor assumption requires that the macroscopic velocity gradient equals its microscopic counterpart. Separating this requirement into the symmetric and skew symmetric parts and removing the volumetric response gives:

$$D'^c = D' \quad (22)$$

and

$$W^c = W, \quad (23)$$

where D and W are the macroscopic deformation rate and spin, respectively. In contrast to the Taylor assumption, when relaxed kinematic constraints are imposed only those components of the deviatoric rate of deformation that lie in the plane of the shared flat grain boundary are required to be the same from crystal to crystal and equal to the macroscopic quantity. Letting n be a vector perpendicular to this plane and m be any vector lying in it (so $n \cdot m = 0$):

$$D'^c \cdot m = D' \cdot m. \quad (24)$$

Furthermore, the tractions on this plane are equal, giving:

$$\sigma'^c \cdot n = \sigma' \cdot n, \quad (25)$$

where σ' is the macroscopic deviatoric Cauchy stress. The deformation rate may vary from crystal to crystal, but must average to the macroscopic value:

$$D' = \frac{1}{N} \sum_c D'^c, \quad (26)$$

where N is the number of crystals in the aggregate [KOC 81, MAT 90b]. An equilibrium-based partitioning can be achieved in a trivial manner by requiring that the stress in every crystal be the same. Because the macroscopic stress is

the average of the crystal stresses, we obtain:

$$\sigma^l = \sigma'^c. \quad (27)$$

This relationship is straightforward to apply if it is the stress that is always known, but more complicated if the macroscopic deformation rate is the known quantity. For the average of the crystal deformation rates to match the macroscopic value, we must also enforce equation [26].³

To complete the link between the microscopic and macroscopic scales the material spin within each crystal must be related to the macroscopic spin. For the Taylor hypothesis, the crystal spin typically is equated to the macroscopic spin. Conceptually, the relaxed constraints model is intended for those instances when crystal are flat and the aggregate can be thought of as layers of thin flat crystals. Throughout the deformation the layers remain parallel. This assumption is accomplished by requiring that the principal axes of the stretch ellipsoids of all crystals under relaxed constraints remain aligned. Based on this requirement, the microscopic spin of a crystal is defined by equating the rate of rotation of the principal axes of the crystal stretch ellipsoid (grain axes) to that of the macroscopic motion:

$$\Omega^c = \Omega, \quad (28)$$

where Ω^c is the microscopic grain axes spin and Ω is the spin of the axes of the macroscopic stretch ellipsoid. For the equilibrium-based assumption, it is possible to apply either of the above rules for determining the crystal spin, with the choice being based on the physical attributes of the system.

4.1 Velocity-pressure formulation

The governing equations which result from balance of momentum and conservation of mass are solved using a finite element discretization of the domain. A weighted residual is formed from the differential form of the equilibrium equation and appropriate weighting functions, ϕ^4 :

$$\int_{\Omega} \phi \cdot (\text{div } \sigma + b) d\Omega = 0 \quad (29)$$

By means of standard finite element techniques, equation [29] may be rewritten as:

$$\int_{\Omega} (\text{grad } \phi) \cdot \sigma' d\Omega - \int_{\Omega} (\text{div } \phi) \cdot p d\Omega = \int_{\Omega} \phi \cdot b d\Omega + \int_{\Gamma} \phi \cdot t d\Gamma \quad (30)$$

³The relative importance of each crystal could be independently weighted if desired without changing the overall structure of the model.

⁴Inertial effects in the momentum balance and elasticity in the material response are neglected here.

where the stress has been split into deviatoric (σ') and volumetric (p) parts, and \mathbf{t} represents the surface traction vector. σ' is eliminated from equation [30] using a viscoplastic constitutive relationship of the form

$$\sigma' = \mathcal{C} : D' \quad (31)$$

where \mathcal{C} is a fourth order stiffness tensor obtained by inverting and averaging the single crystal compliances. This is achieved by forming the weighted average of the crystal level constitutive matrices

$$\mathcal{C} = \sum_c w_c \mathcal{C}^c = \sum_c w_c [\mathcal{M}^c]^{-1} \quad (32)$$

Introducing shape functions for the velocity and pressure fields

$$\mathbf{u} = [N^u]\{U\} \text{ and } p = [N^p]\{P\}, \quad (33)$$

and substituting equation [31] into equation [30] gives

$$\begin{aligned} \int_{\Omega} [B]^T [C] [B] d\Omega \{U\} - \int_{\Omega} [B]^T \{h\} [N^p] d\Omega \{P\} &= \int_{\Omega} [N^u] \{b\} d\Omega \\ &+ \int_{\Gamma} [N^u] \{t\} d\Gamma \end{aligned} \quad (34)$$

or

$$[K]\{U\} - [G]\{P\} = \{f\} \quad (35)$$

This equation is combined with the incompressibility constraint, which appears in an identical manner to the hybrid formulation:

$$[G]^T \{U\} = \{0\} \quad (36)$$

to give the global system of equations:

$$\begin{bmatrix} K & G \\ G^T & 0 \end{bmatrix} \begin{Bmatrix} U \\ -P \end{Bmatrix} = \begin{Bmatrix} f \\ 0 \end{Bmatrix} \quad (37)$$

for the velocity and pressure fields. The resulting matrix equation is nonlinear and is solved with an iterative scheme. This requires information about the mechanical behavior at the integration points for a given estimate for the flow field. For our applications we assume that an aggregate is located within every element of the finite element mesh and that the mechanical behavior can be determined by interrogation of the aggregate. At each iteration on the velocity field, \mathcal{C} is re-computed based on the macroscopic deformation rate and the rule for partitioning that deformation rate among the crystals within the aggregate. The stiffness \mathcal{C} and the deformation rate are then used to eliminate the stress tensor from the weak form of equilibrium and to compute a new estimate for the flow field. As in the case of the hybrid formulation, the presence of the

incompressibility constraint requires special attention in the conjugate gradient procedure [BEA 93].

4.3 Simulation of large-scale processes

The limiting dome height test is used widely to assess the formability properties of metals. The test, shown schematically in Figure 7, consists of stretching a rectangular sheet over a hemispherical punch. The sheet is constrained by a circular drawbead. Because the sheet is rectangular, the extent to which it is constrained by the drawbead is dependent on its width in comparison to the radius of the drawbead. By having a wide sheet, the stress state is near biaxial tension at the punch pole. With a narrow sheet, the stress state is closer to uniaxial.

The effect of processing practice on formability has been reported for an aluminum alloy [BRY 94] in which the measured R-ratio for each rolling practice

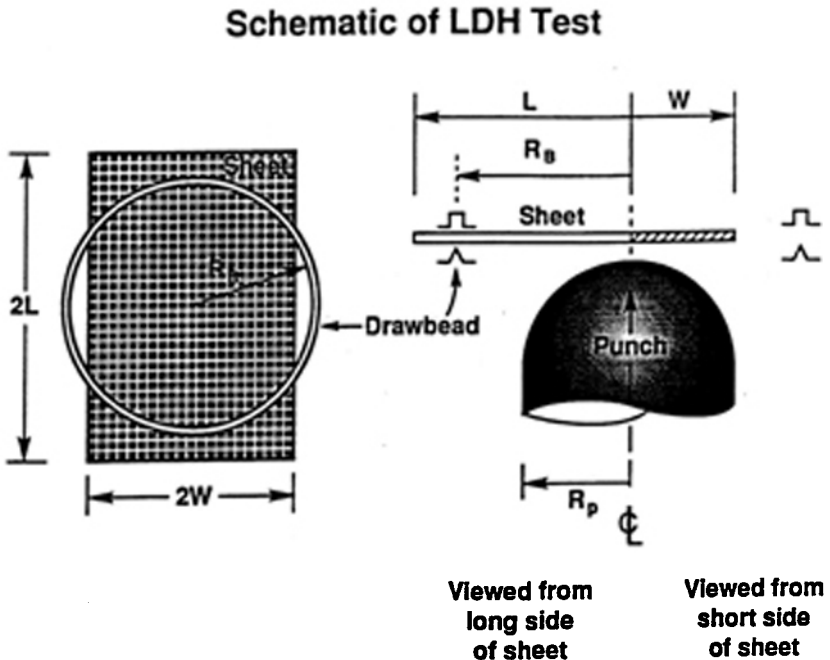


Figure 7: Schematic diagram of limiting dome height test.

has been correlated with its measured dome height prior to failure. The various processing practices induce different crystallographic textures in the sheet, which translate to different initial conditions for the limiting dome height test. Pole figures for two of the practices reported in [BRY 94] are shown in Figure 8.

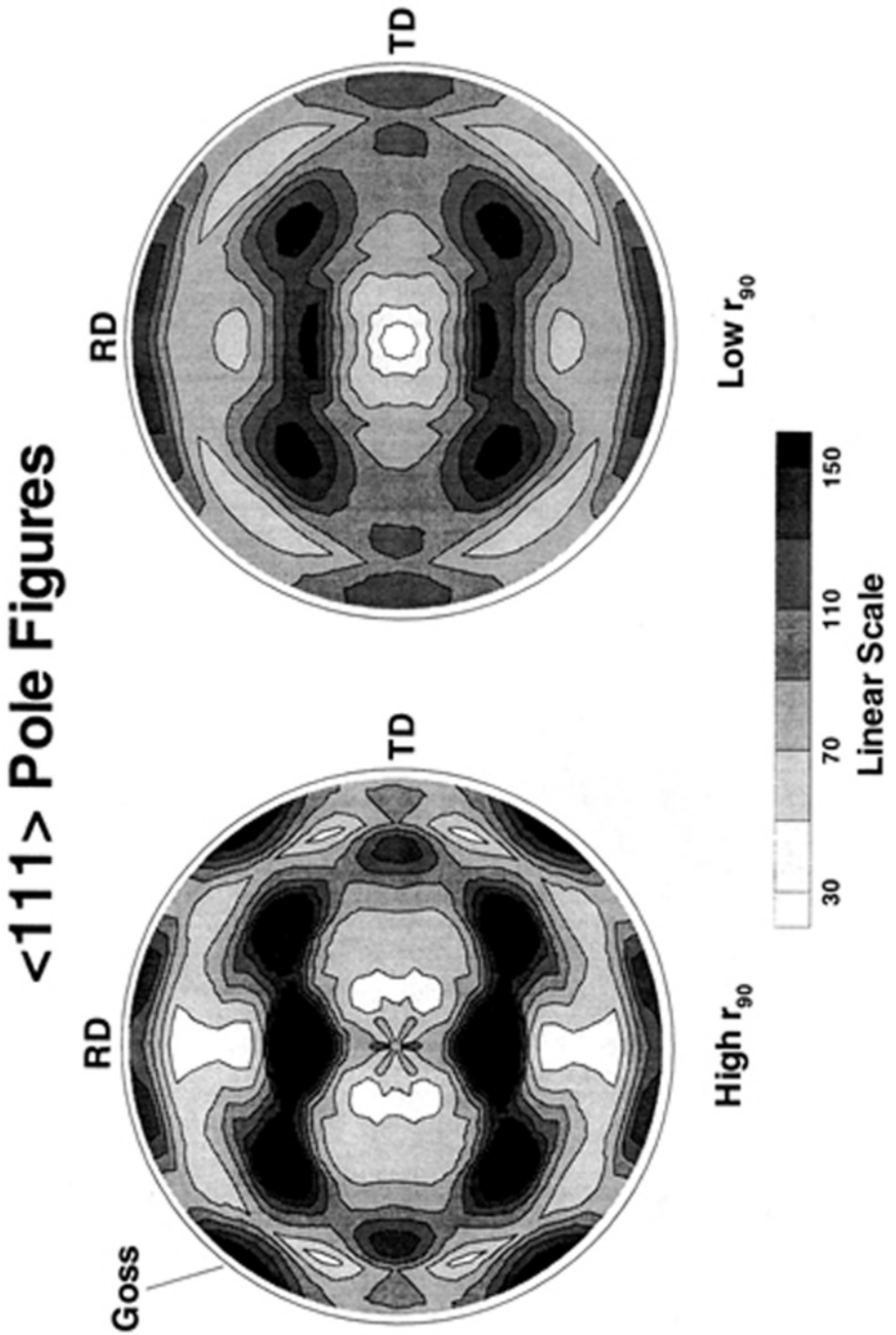


Figure 8: < 111 > pole figures for sheet from two processing practices.

They differ principally in the strength of the Goss component, with greater Goss strength occurring in the sheet with higher measured R-value. The crystallographic texture affects the performance in the limiting dome height test through the effect of anisotropy in plastic flow on the thinning of the sheet.

Simulation of the limiting dome height test was conducted using the large scale velocity-pressure formulation outlined above for initial textures prescribed for the high and low R-value processing practices. The mesh used to discretize a symmetric quarter of the test specimen was comprised of 3600 brick elements, each with an aggregate of 256 weighted crystals. The orientation and weighting of the crystals was determined with the popLA code [KAL 90]. Identical hardening parameters were prescribed for each sheet based on tensile tests performed on samples from the sheet. All test specimens were oriented with the sheet rolling direction corresponding to the long axis of the specimen. Specimens were constrained against movement where they contacted the hold-down tooling; the drawbead was not explicitly modeled. Sticking friction was prescribed for the interface between the punch and the specimen, which corresponded to the unlubricated conditions used in the experiments. The full

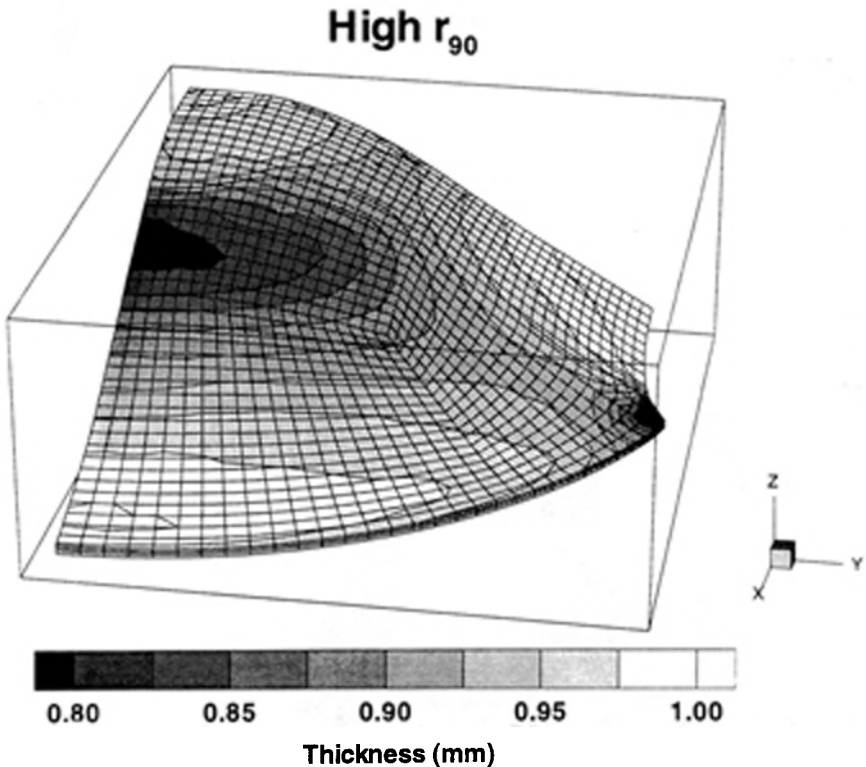


Figure 9: Deformed mesh of the limiting dome height specimen for the case of high R-value sheet. Shading shows thickness contours corresponding to the deformed mesh.

operation was simulated on a CM-5 using 40 time steps.

Shown in Figures 9 and 10 are the deformed meshes for each material, depicting the contours of specimen thickness. The simulation corresponding to the texture having a high R-value shows a greater tendency to thin as the dome height increases. This is consistent with experiments, which show greater dome height with lower R-value. Further, part failures are observed experimentally near the locations of smallest thickness shown in these plots.

5. Implementation issues

Like models for polycrystal plasticity, finite element formulations come in many different forms. Because of this it is not advisable, nor even feasible, to attempt to establish the best wedding of microstructural theory with numerical treatment of a boundary value problem. For example, finite element codes are available based on explicit dynamic formulations as well as implicit static

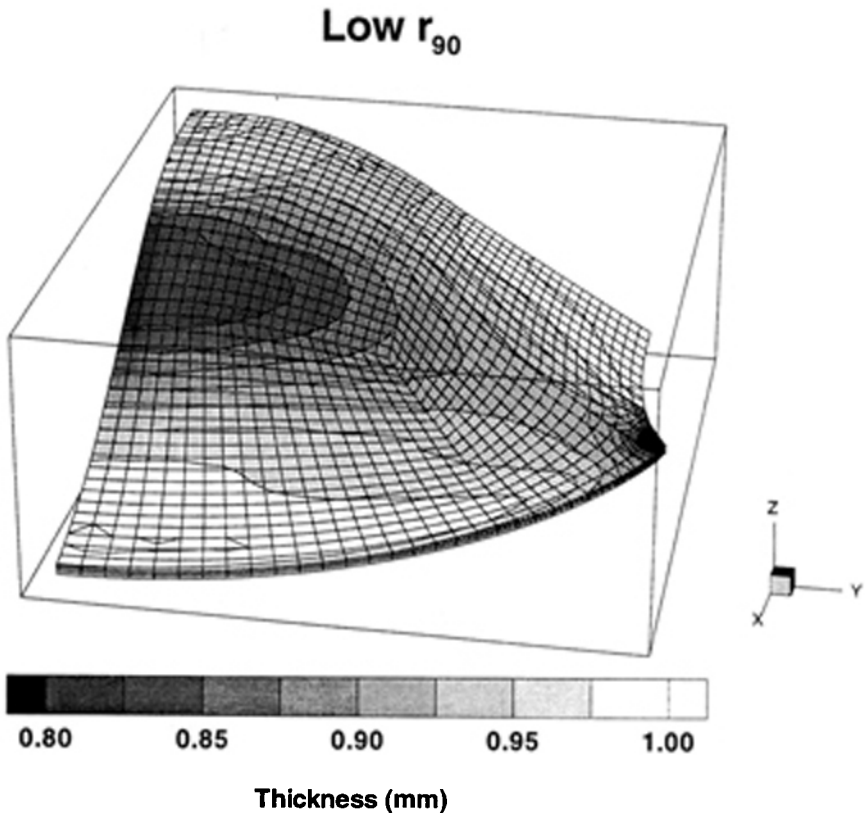


Figure 10: Deformed mesh of the limiting dome height specimen for the case of low R-value sheet. Shading shows thickness contours corresponding to the deformed mesh.

methodologies. Both displacements and velocities have been chosen as the primitive kinematic variables. Some formulations neglect elasticity while others are constructed around its existence. Introduction of a polycrystal plasticity model into a finite element formulation introduces further variants; polycrystal plasticity models have been developed that incorporate an extended Taylor hypothesis while others utilize self consistent premises to allow for richer variety of grain interactions. It is not surprising that various combinations of these have been investigated, nor is it surprising that no single combination has demonstrated clearly its overall superiority.

One special concern arising with formulations that include elasticity is the effective integration of the stress. This involves the crystal kinematics, especially the decomposition of motion in term of elastic and plastic components. Both explicit and implicit procedures have been devised. Peirce, Asaro and Needleman [PEI 83] developed an explicit procedure. Implicit procedures have been reported by Kalidindi, Bronkhurst, and Anand [KAL 92] and by Maniatty, Dawson and Lee [MAN 92].

As a state variable representation for plastic flow, polycrystal plasticity theory has several distinct advantages. Implicit with the use of state variable models is the ability to initialize the state. Orientation distributions are directly accessible via x-ray measurement and well-established methodologies for interpreting those measurements. The crystal hardness distributions are not as direct, but for the restricted assumption of common hardening among all crystals of an aggregate the hardness may be initialized from simple compression testing. Polycrystal theory also provides a direct means for updating the material state via integration of the evolution equations for the crystal lattice orientation and the hardness.

In large scale applications, the aggregate is not a body, but rather only an abstract representation of the microstructural state. Care must be exercised in assuring consistency between the macroscopic material element size and the aggregate dimensions. It is possible to think of macroscopic deformation gradients within the workpiece that are large, yet only vary slowly across the dimension of an aggregate. As such we may consider the aggregate to be subjected to a uniform deformation locally. Locally here refers to a point on macroscopic scale, so that we permit only single (tensor) values of stress and velocity gradient. Thus the dimension of a crystal must be small compared to the dimension over which the macroscopic velocity gradient changes appreciably. In turn, the aggregate of crystals must contain a sufficient number and inherent appropriate symmetry relations such that the above arguments of homogenization are justified.

In most finite element implementations, isoparametric elements are employed in which gradients of velocity (or displacement) may exist across an element. Further, elemental integrations are performed using quadrature in which the integrand is evaluated at specific points within an element. One can consider the material in the vicinity of a quadrature point as a region on which

the homogenization is performed on the crystal responses of an aggregate. Sufficient crystals must reside in this region for the homogenization to be valid, as discussed in the previous paragraph. Variations in the velocity gradient within an element imply, however, that all of the quadrature points are not experiencing the same strain rate. The material's rate sensitivity, texture, and hardening characteristics become important then because of the influence they exert on the variations in stress in the presence of differences in the strain rate over the domain of the element. For convergence of the finite element solution for the motion, the stress should approach a smooth distribution within an element and across its boundaries to neighboring elements. Smoothness of stress will not be achieved without some smoothness of the properties. This requires that the number of crystals within an aggregate be sufficiently large to represent an orientation distribution well, and that the distributions within an element not vary greatly. In fact, the use of a single aggregate within each element, placed at its centroid, provides excellent performance in finite element simulations because it restricts the possible variations of stress. For consistency then, as elements become sufficiently small that smooth stresses are achieved, they each must still remain sufficiently large to physically contain an aggregate that is representative of the complete distribution and over which a legitimate homogenization may be performed.

6. Parallel Computing Strategies

Finite element formulations that employ polycrystal plasticity model are computationally demanding. If a large scale application is pursued on a single processor computer architecture the calculations related to the crystal equations can take up to 95% of the execution time. For these models the materials related computations dominate. This is a switch in the primary computational demand in finite element model from most of the resources being consumed satisfying the balance laws to most of the resources being used for materials related computations. However, parallel computer architectures are ideal for these models as they contain a high degree of concurrency.

The parallel implementation of the mathematical formulation discussed here consists of three independent data structures: a set of unassembled finite elements; a set of assembled nodal degrees of freedom; and a set of crystals. Any interaction between the three data structures results in communication between the processing nodes of the parallel architecture. These three data-sets must be mapped to the processing nodes of the parallel architecture such that there is arithmetic load balance, the locality of reference is maximized, and the contention for the communication channels in the network interconnecting the processing nodes is kept to a minimum.

The finite elements in the mesh are grouped into sub-meshes for mapping to the processing nodes using a parallel implementation of the recursive spectral bisection algorithm [JOH 94a, JOH 94b, TMC 94]. No assumptions are made

regarding the topology of the mesh. The mapping obtained by this algorithm attempts to maximize the locality of the sub-mesh residing on each processing node by ensuring that the finite elements comprising the sub-meshes are geometrically connected and have a surface area to volume ratio that is close to optimal.

Nodal points that are interior to the sub-mesh residing on a processing node are mapped to that same processing node. Boundary nodes must be assigned to one of the processing nodes with which they are associated, or replicated on all of the processing nodes in which they appear. Only boundary nodes necessitate communication. The implementation reported here assigns the boundary nodes to one of the partitions with which they are associated in a random manner. Randomization minimizes the contention for the communication channels that interconnect the processing nodes [VAL 82].

The finite element formulation outlined earlier permits an arbitrary number of crystals in each element. For the case of one crystal per element, the crystals are mapped to the processing nodes using the same mapping as the finite elements. For the case when the crystal to element ratio is greater than one [BEA 93], the set of crystals is viewed as a two-dimensional data set (a dense matrix). The rows of the matrix represent the crystals with an aggregate and the columns of the matrix represent the aggregate. The number of aggregates (= number of columns) is the same as the number of finite elements (N_e) comprising the finite element mesh. The number of rows is the crystal to element ratio (N_c). The data interaction between the set of unassembled finite elements and crystals involves broadcast and reduce operations. A broadcast is necessary for replicating the aggregate values to the individual crystals comprising the aggregate. A reduce operation is necessary to average the data values of individual crystals within an aggregate. Both the broadcast and reduce operations must exploit parallelism within the rows and columns of the two-dimensional data-set. A blocked (consecutive) mapping scheme ensures an optimal layout for the parallel broadcast and reduce operations. The group of crystals reside in an array of shape $N_c \times N_e$. The local sub-array on each processing node is of the shape $\lceil \frac{N_c}{P_1} \rceil \times \lceil \frac{N_e}{P_2} \rceil$, where P_1 and P_2 are the number of processing nodes along the two axes ($P_1 \times P_2 = P$ and P is the number of processing nodes).

All the finite element meshes that are used in the simulations reported here are comprised of one type of element only. The arithmetic operation count for each crystal is almost uniform. Consequently, there is near perfect arithmetic load balance for all element-wise computations. The blocked mapping scheme results in an even distribution of the crystals on the processing nodes. This is sufficient for achieving arithmetic load balance without sophisticated data dependence.

Concurrency is exploited at the level of unassembled finite elements, assembled nodal points and crystals. The crystal behavior equations (equation [16]) and the nodal stress–nodal velocity relation (equation [18]) are solved/inverted concurrently for all the crystals in the aggregate. The unassembled element-wise matrices in equation [20] are evaluated concurrently for all finite elements in the mesh. The resulting sparse linear system (equation [20]) is solved using a conjugate gradient method; no explicit assembly of the sparse coefficient matrix is required. The poor condition of the coefficient matrix caused by the incompressibility constraint (equation [21]), however, requires special treatment [BEA 94].

7. Summary

Finite element formulations that utilize polycrystal plasticity as the constitutive description have progressed significantly over the past decade. Gains have been reported both in the use of polycrystal descriptions to better understand fundamental aspects of the deformation behavior of crystalline solids and in the investigation of commercial forming operations for these materials. While considerable progress has been made, a variety of issues remain open as to the best way to merge the two. The relative size of crystals and elements plays an important role in this respect. In all cases, the computational demands are heavy, but the opportunity for concurrency is great. Formulations can exploit this concurrency with implementations designed for massively parallel computer architectures.

Acknowledgements

This work was supported through the Office of Naval Research under contract NOO014-90-J-1810. Access to computing resources was provided by the Advanced Computing Laboratory at Los Alamos Laboratories and the National Center for Supercomputing Applications at the University of Illinois.

References

- [ASA 85] ASARO, R.J. and NEEDLEMAN, A., Texture Development and Strain Hardening in Rate Dependent Polycrystals, *Acta Metall.*, 23, 1985, p. 923–953.
- [ATL 75] ATLURI, S.N., On 'hybrid' finite element methods in solid mechanics, *Advances in Computer Methods for Partial Differential Equations*, R. Vichnevetsky (ed.), Publ. AICA, 1975.
- [BEA 93] BEAUDOIN, A.J., MATHUR, K.K., DAWSON, P.R. and JOHNSON, G.C., Three-dimensional deformation process simulation with explicit use of polycrystalline plasticity models, *Int. J. Plast.*, 9, 1993, p. 833–860.

- [BEA 94] BEAUDOIN, A.J., MATHUR, K.K., DAWSON, P.R. and KOCKS, U.F., A Hybrid Finite Element Formulation with Consideration of Macrostructural and Microstructural Linking, *Int. J. Plast.*, in press.
- [BEC 91a] BECKER, R., Analysis of texture evolution in channel die compression - I. Effects of grain interaction, *Acta Metall. Mater.*, 39, 1991, p. 1211-1230.
- [BEC 91b] BECKER, R., Modeling Def. Crys. Solids, TMS, 1991, p. 249.
- [BRA 83] BRATIANU, C. and ATLURI, S.N., A hybrid finite element method for Stokes flow: Part I - formulation and numerical studies, *Comp. Meth. Appl. Mech. Engrg.*, 36, 1983, p. 23.
- [BRY 94] BRYANT, J.D., BEAUDOIN, A.J. and VANDYKE, R.T., The Effect of Crystallographic Texture on the Formability of AA 2036 Autobody Sheet, SAE Technical Paper Series, 940161, 1994.
- [CHA 91] CHASTEL, Y.B. and DAWSON, P.R., Comparison of polycrystalline rolling simulations with experiments, *Modeling Def. Cry. Solids (TMS)*, 1991, p. 225-238.
- [CHA 93a] CHASTEL Y.B. and DAWSON, P.R., An Equilibrium Based Model for Anisotropic Deformations of Polycrystalline Materials, *Proc. ICOTOM-10*, Clausthal, Germany, 1993, p. 1747-1752.
- [CHA 93b] CHASTEL, Y.B., DAWSON, P.R., WENK, H.-R. and BENNETT, K., Anisotropic Convection with Implications for the Upper Mantle, *J. Geophys. Res.*, 98, n.B10, 1993, p. 17757-17771.
- [DAW 92a] DAWSON, P.R., BEAUDOIN, A.J. and MATHUR, K.K., Simulating deformation-induced texture in metal forming, *Numerical Methods of Industrial Forming Processes, NUMIFORM '92*, Rotterdam, 1992, p. 25-33.
- [DAW 92b] DAWSON, P.R., BEAUDOIN, A.J., MATHUR, K.K., KOCKS, U.F. and KORZEKWA, D.A., Crystallographic texture effects in hydroforming of aluminum sheet, *Num. Meth. Sim. Ind. Metal Forming Proc.*, ASME-AMD, 156, 1992, p. 1-10.
- [DAW 93] DAWSON, P.R., CHASTEL, Y.B., SARMA, G.B. and BEAUDOIN, A.J., Simulating Texture Evolution in Fe-3%Si with Polycrystal Plasticity Theory, *Proc. Int. Conf. Modeling Metal Rolling Processes*, The Institute of Materials, London, 1993.
- [DAW 94] DAWSON, P.R., BEAUDOIN, A.J., and MATHUR, K.K., Finite element modeling simulations of polycrystals, *Computational Material Modeling*, A. Noor (Ed.), ASME, in press.
- [GOT 78] GOTOH, M., A finite element formulation for large elastic-plastic deformation analysis of polycrystals and some numerical considerations on polycrystalline plasticity, *Int. J. Num. Meth. Engrg.*, 12, 1978, p. 101-114.
- [HAR 89] HARREN, S.V. and ASARO, R.J., Nonuniform deformations in polycrystals and aspects of the validity of the Taylor model, *J. Mech. Phys. Solids*, 37, 1989, p. 191-232.

- [HAV 92] HAVLICEK, F., TOKUDA, M., HINO, S. and KRATOCHVIL, J., Finite Element Analysis of Micro-Macro Transition in Polycrystalline Plasticity, *Int. J. Plast.*, 8, 1992, p. 477-499.
- [HON 78] HONEFF, H. and MECKING, H., A method for the determination of the active slip systems and orientation changes during single crystal deformation, *Textures of Materials, Proc. ICOTOM V, Berlin, 1978*, p. 265.
- [HON 84] HONEYCOMBE, R.W.K., *The Plastic Deformation of Metals*, 2nd Ed., Edward Arnold, London, 1984.
- [HUT 77] HUTCHINSON, J.W., Creep and plasticity of hexagonal polycrystals as related to single crystal slip, *Metall. Trans.* 8A, 1977, p. 1465-1469.
- [JOH 94a] JOHAN, Z., MATHUR, K.K., JOHNSON, S.L. and HUGHES, T.J.R., An Efficient Communication Strategy for Finite Element Methods on the Connection Machine AM-5 System, *Comp. Meth. Appl. Mech. and Engrg.*, 113, 1994, p. 363-387.
- [JOH 94b] JOHAN, Z., MATHUR, K.K., JOHNSON, S.L. and HUGHES, T.J.R., Scalability of Finite Element Applications on Distributed-memory Parallel Computers, *Comp. Meth. Appl. Mech. and Engrg.*, in press.
- [KAL 90] KALLEND, J.S., KOCKS, U.F., Rollett, A.D. and WENK, H.-R., Operational Texture Analysis, *Mater. Sci. Engrg.*, A123, 1991, p.1-11.
- [KAL 92] KALIDINDI, S.R., BRONKHORST, C.A. and ANAND, L., Crystallographic texture evolution in bulk deformation processing of fcc metals, *J. Mech. Phys. Solids*, 40, 1992, p. 537-569.
- [KOC 70] KOCKS, U.F., The Relations between Polycrystal Deformations and Single Crystal Deformations, *Metall. Trans.*, 1, 1970, p. 1121-1143.
- [KOC 81] KOCKS, U.F., and CANOVA, G.R., How many slip systems and which ?, *Deformation of Polycrystals*, Riso National Laboratory, Roskilde, Denmark, 1981, p. 35.
- [LEB 94] LEBENSON, R.A., SANCHEZ, P.V. and POCHETTINO, A.A., Modeling Texture Development of Zirconium Alloys at High Temperatures, *Scripta Metall. et Mater.*, 30, 1990, p. 481-486.
- [MAN 91] MANIATY, A.M., Ph.D. Dissertation, Cornell Univ., 1991.
- [MAN 92] MANIATY, A.M., DAWSON, P.R. and LEE, Y.S., A time integration algorithm for elasto-viscoplastic cubic crystals applied to modeling polycrystalline deformation, *Int. J. Num. Meth. Engrg.*, 35, 1992, p. 1565-1588.
- [MAT 89] MATHUR, K.K. and DAWSON, P.R., On modeling the development of crystallographic texture in bulk forming processes, *Int. J. Plast.*, 5, 1989, p. 67-94.
- [MAT 90a] MATHUR, K.K. and DAWSON, P.R., Texture development during wire drawing, *J. Engrg. Mat. Tech.*, 112, 1990, p. 292-297.
- [MAT 90b] MATHUR, K.K., DAWSON, P.R. and KOCKS, U.F., On modeling anisotropy in deformation processes involving textured polycrystals with distorted grain shape, *Mech. Mater.*, 10, 1990, p. 183-202.

- [MCH 93] MCHUGH, P.E., ASARO, R.J. and SHIH, C.F., Computational modeling of metal matrix composite materials – I. Isothermal deformation patterns in ideal microstructures, *Acta Metall. Mater.*, 41, n.5, 1993, p. 1461–1476.
- [NEE 85] NEEDLEMAN, A., ASARO, R.J., LEMOND, J. and PEIRCE, D., Finite element analysis of crystalline solids, *Comp. Meth. Applied Mech. Engr.*, 52, 1985, p. 689–708.
- [PEI 83] PEIRCE, D., ASARO, R.J. and NEEDLEMAN, A., An analysis of nonuniform and localized deformation in ductile single crystals, *Acta Met.*, 30, 1982, p. 1087–1119.
- [SME 91] SMELSER, R.E. and BECKER, R., Earing in cup drawing of a (100) single crystal, *ABACUS User's Group Conf. Proc.*, Oxford, 1991, p. 457–471.
- [TMC 94] CMSSL for CM-Fortran: CM-5 Version, Version 3.1, Thinking Machines Corporation, 1994.
- [TOM 84] TOME, C., CANOVA, G.R., KOCKS, U.F., CHRISTODOULOU, N. and JONAS, J.J., The relationship between macroscopic and microscopic strain hardening in fcc polycrystals, *Acta Metall.* 32, 1984, p. 1637–1653.
- [TOM 91] TOME, C., LEBENSOHN, R.A, KOCKS, U.F., A model for texture development dominated by deformation twinning: application to zirconium alloys, *Acta Metall. Mater.*, 39, 1991, p. 2667–2680.
- [TON 69] TONG, P. and PIAN, T.H.H., A variational principle and convergence of a finite-element method based on assumed stress distribution, *Int. J. Solids Struct.*, 5, 1969, p. 463.
- [VAL 82] VALIANT, L., A Scheme for Fast Parallel Communication, *SIAM J. Comp.*, 11, 1982, p. 350–361.
- [VAN 91] VAN BAELE, A., VAN HOUTTE, P., AERNOUDT, E., HALL, F.R., PILLINGER, I., HARTLEY, P. and STURGESS, C.E.N., Anisotropic finite-element analysis of plastic metalforming processes, *Textures and Microstructures*, 14–18, 1991, p. 1007–1012.
- [YAO 93] YAO, Z. and WAGONER, R.H., Active slip in aluminum multicrystals, *Acta Metall. Mater.*, 41, n. 2, 1993, p. 451–468.

Appendix

Matrices used in the finite element discretization are given below.

$$[R] = \int_{\Omega_e} [B]^T [N^\sigma] d\Omega$$

$$[G] = - \int_{\Omega_e} [B]^T \{h\} [N^p] d\Omega$$

$$\{f\} = \int_{B_e} [N^u]^T \{t\} dB$$

$$[H^e] = \int_{\Omega_e} [N^\sigma]^T [S^e] [N^\sigma] d\Omega$$

$[B]$ is the usual matrix containing the gradient of the velocity shape functions, $\{t\}$ is the vector representation of the tractions \mathbf{t} , and $\{h\}$ is a vector form of the trace operator.